Journal of Applied Fluid Mechanics, Vol. 15, No. 5, pp. 1387-1401, 2022.
Available online at www.jafmonline.net, ISSN 1735-3572, EISSN 1735-3645.
https://doi.org/10.47176/jafm.15.05.33448

Evaluation of CFD URANS Turbulence Models for the Building under Environmental Wind Flow with Experimental Validation

K. B. Rajasekarababu[1†], G. Vinayagamurthy[1] and S. Selvi Rajan[2]

[1]*School of Mechanical Engineering, (Aerodynamics laboratory), VIT-University Chennai -600127, India*
[2]*CSIR-SERC (Wind engineering laboratory)/ NeXHS, Chennai-600113, India*

†*Corresponding Author Email: kbrajasekarababu@klu.ac.in*

(Received October 7, 2021; accepted April 24, 2022)

ABSTRACT

Wind flow on and around buildings attains more importance among architectures, builders, urban planners, structural engineers, and wind engineers. Wind tunnel experiments and wind flow assessments of full-scale buildings are expensive and complex in varied terrain conditions. Hence, wind flows are extensively assessed using Computational Fluid Dynamics (CFD). By following the turbulence parameters, CFD turbulence models create the wind tunnel and atmospheric environments. No literature has till elucidated which CFD turbulence model is more suitable for predicting the terrain wind flow on and around high-rise buildings. The efficiency of the CFD models, their performance, and their accuracy must be validated with experimental results, which is indispensable before using the turbulence model in practice. Therefore, this investigation aims to validate the Unsteady Reynolds–Averaged Navier-Stokes (URANS) simulations for a setback tall building under open terrain wind conditions enclosed within the wind tunnel dimensions. The URANS simulation is accompanied with Standard k– ε, Realizable k-ε, RNG k-ε, Standard k–ω, k–ω SST and RSM. The k –ω SST and RSM turbulence models have reproduced the wind pressure coefficients observed from the wind tunnel. However, all turbulence models failed to produce the same velocity profiles at downstream recirculation, as they vary with sampling time. The transient feature, RMS (Root Mean Square), is better reproduced by RSM and k–ω SST models, while the most unsteady features like across wind spectra and eddies were captured by Realizable, RSM and SST using iso-surface. k–ω SST and RSM models predict similar results with the experiment. Where less computational time was required for the SST, it is promising that this model provides both mean pressure and unsteady feature, encouraging more accurate simulation around the buildings.

Keywords: CFD turbulence models; URANS; Wind pressure coefficients; Iso-surface; CFD; Terrain wind flow; Setback building; Aerodynamic coefficients.

NOMENCLATURE

ABL	Atmospheric Boundary Layer	TKE	Turbulence Kinetic Energy
		$u_i(t)$	instantaneous velocity
AIJ	Architectural Institute of Japan	$u_i'(t)$	turbulent fluctuations
CFD	Computational Fluid Dynamics	$\overline{u_i}$	mean velocity
CSIR-SERC	Council of Scientific and Industrial Research-StructuralmEngineering Research Centre.	SIMPLE	Semi-Implicit Method for Pressure-Linked Equations
C_D	drag coefficient	$\tilde{u}_i$	periodic fluctuation
C_L	lift coefficient	U_H	velocity at the reference height
Cp_{Mean}	mean pressure coefficient	u^*_{ABL}	frictional velocity of ABL
Cs	roughness constant	y_0	length of the roughness
F_D	force in the streamwise direction	ε	turbulence energy dissipation
F_L	force in a transverse wise direction	κ	Karman constant
K_s	sand grain roughness height	t*	length of the sampling time

LES	Large Eddy Simulation
$\bar{p}$	mean pressure obtained for a time
$\tilde{p}$	fluctuating pressure
RANS	Reynolds-averaged Navier–Stokes
SRANS	Steady Reynolds-averaged Navier–Stokes

1. INTRODUCTION

The effects of wind are closely related to wind load and natural ventilation in the environment around buildings. Therefore, tall buildings are extremely challenging due to three-dimensional flow structures comprising of an wide radius of flow regimes like recirculation, stagnation and wake zones. Even for a simple, small building geometry, the flows can be complex demanding a thorough investigation of the upstream and downstream flow features (external wind environment) as well as pressure distributions around it. Thus,it is difficult to extract and capture these flow features with experimental measurement methods and more challenging to quantify precisely by Joubert *et al.* (2015).

CFD has also been used to understand the wind flow features around the buildings like pedestrian comfort, wind loads, inference effects, microclimate effects and pollution dispersion in the building environments by Mochida and Lun (2008), Blocken *et al* (2011), Blocken *et al.* (2012), Tominaga and Stathopoulos (2013). Conditions and parameters must agree with the guidelines since CFD outputs primarily depend on various turbulence and inlet conditions. Casey and Wintergerste *et al.* (2002), Franke *et al*. (2007), Blocken *et al.* (2012) drafted computational wind engineering best practice guidelines. The turbulence model's choice is significant to simulate the wind flow features because it affects the flow variables(pressure, velocity, TKE, streamline patterns etc.). Hanjalić and Kenjereš (2008) have imparted that the turbulence model selection should be given primary care. The LES and RANS are the renowned turbulence models used to predict the wind pressure and flow on and around the building. Since the equations are resolved in steady-state approximations, RANS models are known as SRANS and are used in almost all engineering applications. In practice, the wind flow is unsteady (instantaneous random fluctuations) due to the turbulence's large-scale, periodic, unexpected motion. The triple decomposition method's instantaneous velocity can be disintegrated, as suggested by Hussain and Reynolds (1970). Decomposition is as follows:

$$u_i(t) = U_i + u_i'(t)$$
$$U_i = \bar{u}_i + \tilde{u}_i \quad (1)$$

Here, $u_i(t)$ is the instant wind velocity, $u_i'(t)$ is turbulent fluctuations, $\overline{u_i}$ is the mean velocity, $\tilde{u}_i$ is the periodic fluctuation, the time -averaged velocity U_i. Here in equation (1), U_i is resolved by transient scheming and therefore called URANS. The contribution of the ratio of periodic fluctuations and total fluctuations depends on flow characteristics and the use of SRANS. A few researchers have applied URANS models to flow fields around typical buildings exposed to high turbulence. Rahmatmand *et al.* (2014) chose the RNG k-ε model to measure turbulent airflow around a domed-roof building and exhibited the vortices, shear layer, and velocity profiles around the building. Vatin *et al.* (2014) state that the framework of URANS enables the estimation of vortex structures size and reveal the flow mechanism by improved inlet boundary conditions. Zhang *et al.* (2015) studied the flow around super-tall structures using the RSM model. The closeness of results with experimental values concludes that the RSM model can simulate the wind flow efficiently. Tominaga (2015) observed that k–ω SST model among (standard k–ε, realizable k–ε, RNG k–ε, k–ω SST and standard k–ω) other URANS models reproduces the unsteady fluctuations in the downstream wind flow. They concluded that among the URANS family, the modified ε equation in RNG k–ε demonstrated low discrepancies with the experiment. Tall buildings exhibit considerable influence on microclimates such as wind flow, heat transfer and shadow effect. From the CFD simulations, the impact of climate changes can be evaluated by appropriate deterministic boundary conditions. Toparlar *et al.* (2015) analyzed the urban microclimate changes (wind flow and heat transfer) using the Realizable k–ε turbulence model. They achieved good agreement with satellite imagery data with a maximum average deviation of 7.9%. Tominaga (2015) studied the steady and unsteady RANS model and obtained the unsteady flow features around the building using five URANS turbulence models. However, they did not include the power spectra of the across wind flow. The force coefficients are also an important parameter to understand the flow features around buildings. Surface pressure and force coefficients on Z-plan shaped buildings for different wind angles of incidences using the k-ε model was computed by Paul and Dalui (2016). Iqbal and Chan (2016) studied the wind flow environment around a set of cross-shaped high-rise building by calibrating the closure functions and damping coefficients in standard k–ε model to examine the prediction of flow near-wall region. Yuan *et al.* (2017) analyzed the aerodynamic force coefficients and wind environment around an L-shaped building using the RSM model. Zhang (2017) detailed the performce outcomes of two LES methods and eight RANS turbulence models uing circular cylinder with Aspect Ratio of 1.0 under Re.no of 20,000, the unsteady flow features and time averaged streamline wind profiles on respective planes were examined, the k-ω-SST model showed excellent general results. LES and RANS were later reviewed

by Blocken (2018) for indoor-outdoor applications, and (U)RANS results were found to be sufficiently accurate. Rajasekarababu *et al.* (2016a ; 2019b) detailed the flow features around a setback structure using hybrid turbulence models (DDES & IDDES). Their study concluded that the IDDES model predicts both RMS and mean wind pressure CFD results well w.r.t experimental results. Li *et al.* (2019) investigated six turbulence models to apply aerodynamic behaviour in crosswinds of trains. They found that the k-ω SST would be appropriate for numerical simulation for aerodynamic problems. Rajasekarababu and Vinayagamurthy (2020) discussed the effects of upstream terrain characteristics in aerodynamic coefficient on building using CFD. In Yagmur *et al.* (2020),examined the mean wind flow characteristics like velocity streamline patterns, TKE, drag coefficients, stress correlations and pressure are evaluated using RANS, DES and LES models using a semi-circular cylinder. Their results showed that SST, Realizable & standard derivatives of k-ε models exhibited comparable results with experiments. Hassan *et al.* (2021) investigated the turbulent wake around a building using realizable k-ε turbulence model. They designed an inflow condition that improves accuracy and addressed the reversed flows in the outlet. No literature has explained the choice of the URANS model for predicting the terrain wind flow on and around a building. There is no universally valid turbulence model either. Even minor changes in the building geometry can influence the flow pattern, thereby changing the turbulence model choice. CFD turbulence models can only be evaluated after showing that computational errors are sufficiently small, quantifiable, or negligible. This evaluation of wind flow including wind flow patterns, upstream stagnation, downstream recirculation, surface pressure distribution, across wind spectra, mean aerodynamic coefficients, iso-surface, and TKE on and around the building would assist in selecting the turbulence model for environmental wind flow. Furthermore, user can choose the turbulence model for their required variable. Besides the above-mentioned flow characteristics, the effect of setbacks has also been evaluated. Several CFD tools are available and utilized in these aspects but require proper benchmark validation for reliability. Accordingly, this study aims at observing the performance and accuracy of six URANS models on setback building.

2. METHODOLOGY

2.1 Description of the Set-up

In this study, the chosen setback tall building consists of a roof and three setbacks with two criteria: The side ratio of the building is 1:1.5 & the area ratio of the roof and base-floor is 0.16 for three equally segmented consecutive levels. The real-scale height of the building is 210 m. To simulate open terrain environmental wind flow in the wind tunnel, a geometric scale of 1/300 rigid prototype model has been fabricated using an acrylic sheet, as shown in Fig. 1. The geometrically scaled model dimensions are: height *(H)* =0.7 m with the base-floor area 0.15 m × 0.1 m and the following floor areas are 0.12 m × 0.08 m, 0.09 m × 0.06 m and 0.06 m × 0.04m model is shown in Fig. 2.

Fig. 1. *(*a) Side view of ABL wind tunnel at CSIR-SERC (b) Setback structure inside the wind tunnel test section.

2.2 Testing in a Wind Tunnel

Wind tunnel measurements for the model of setback building have been acquired from wind engineering lab CSIR-SERC Chennai, India (Fig. 1(a)). Dimensions of the open-circuit Atmospheric Boundary Layer Wind Tunnel (ABLWT) test section and blockage ratio is 2.5 m × 2.1 m × 18 m and 2.3%, respectively. According to Tominaga *et al.* (2008), for practical CFD applications like pedestrian comfort, the maximum permissible value of blockage ratio is 5% as per the AIJ guidelines. The setback building model is tested by simulating open terrain wind flow at a time averaged wind speed of U_{mean} = 13.6 m/s and 10 - 11 % of turbulence intensity (I) at the height of the structure. The pitot values are acquired from the undisturbed upstream wind flow from iniside the test section. The pressure ports are located at different heights: y/H=0.225, y/H=0.475, y/H= 0.625 and y/H= 0.875 throughout the perimeter of the structure and the pressure data was recorded 800 Hz sampling rate for 13 seconds to represent the mean hourly wind in the full-scale building. The instrumented (scanner, pressure tapings) building model inside the test section as demonstrated in Fig. 1(b).

2.3 Computational Domain and Grid Generation

Both the computational domain (see Fig. 2) and the wind tunnel test section are the same. Open terrain profile is deployed in the domain to ensure a fully

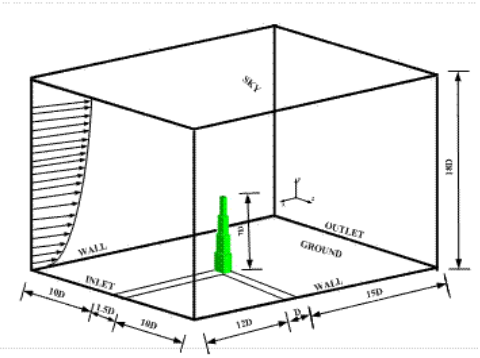

Fig. 2. Perspective view of the wind tunnel test section as a computational domain and setback model dimensions.

developed flow as per Franke *et al.* (2007). According to Blocken *et al.* (2007), the wall distance should be higher than roughness height (Δx ≥ Ks) for creating open terrain profile. Therefore, the roughness height used is 0.0019m, and the first element cell height at the wall is 0.00195 m. The computational grid (a fully structured hexahedral cell of expanding ratio 1.12) is constructed using ICEM-CFD, as shown in Fig. 3 (a). As in Table .1, the grid independence test was performed using three grids: Grid-A (coarse), Grid-B (medium), and Grid-C (fine) grids. The grid sensitivity study was conducted using the k–ω SST model to determine the accuracy and time required to compute the results. Fig. 3 (b) shows the grid independence results.

Table 1. Grid resolution size and elements

Grid resolution	Δ_x (m)	No. Elements
Coarse (Grid A)	0.00200	3657335
Medium (Grid B)	0.00195	5346015
Fine (Grid C)	0.00190	6468468

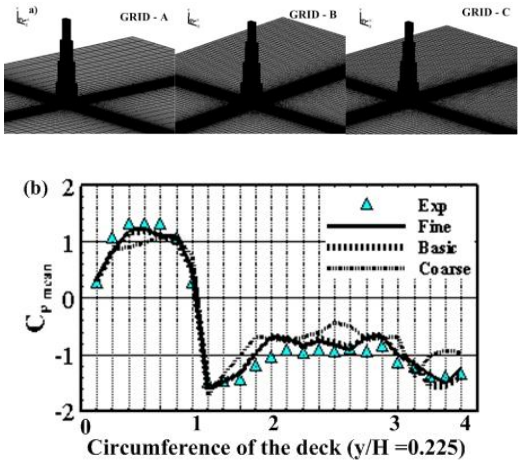

Fig. 3. (a) Perspective view of the three grids and domain (b) Comparison of mean pressure coefficients for the three grids.

3. GENERATION OF ATMOSPHERIC BOUNDARY LAYER

3.1 Turbulence Models and Boundary Conditions

Six turbulence models, i.e., Standard k– ε, Standard k–ω, k–ω SST, Realizable k-ε, RNG k-ε, and RSM models are used for computational simulation Fluent ANSYS (2017). The inlet boundary conditions and turbulence parameters for both thecomputational simulation and wind tunnel measurements were kept same which follows the below equations.

$$(U_y) = \frac{u^*_{ABL}}{\kappa} \ln\left(\frac{y + y_o}{y_o}\right) \tag{2}$$

Logarithmic law [Eq. (2)] is used to define the inlet wind velocity profile, where y_0 = 0.0001 m, u^*_{ABL} is the frictional velocity of ABL, κ is the Von Karman constant (0.40), and y is the vertical coordinate of inlet boundary domain. The turbulent intensity *(I)* is the significant factor for the wind flow characteristic and is calculated using Eq. (3)

$$I(y) = \frac{1}{\ln\left(\frac{y}{y_0}\right)} \tag{3}$$

In the initial conditions, the TKE *(k)* is estimated from the time averaged wind velocity and the turbulence intensity *(I)* by using Eq. (4), where *I(y)* indicates intensity of the turbulence in streamwise direction. The parameter, *a*, can ranges from 0.5 to 1 (Here, a is chosen as recommended by AIJ guidelines (*a* = 1) Mochida *et al.* (2002).

$$k(y) = a(I(y)(U_y))^2 \tag{4}$$

Eq. (6 and 5) respectively calculates the specific dissipation rate *ω(y)* and the turbulence dissipation rate *ε(y)*, where empirical constant, *Cμ*, is set to 0.0845 for RNG and 0.09 for remaining simulation (only for inflow conditions). The Reynolds-Stress Specification method is used in the RSM model as *k* or turbulence kinetic energy.

$$\varepsilon(y) = \frac{u^{*3}}{\kappa(y + y_0)} \tag{5}$$

$$\omega(y) = \frac{\varepsilon(y)}{C\mu k(y)} \tag{6}$$

Following Cebeci and Bradshaw (1977), Launder and Spalding (1974) recommended the standard wall function with modified roughness. This is used for the ground surface. The constant roughness parameter values *(Cs)* were defined using their uniformity correlation with aerodynamic roughness length y_0 is obtained from Blocken *et al.* (2007) for ANSYS FLUENT-19.5, Eq. (7). The values of *Ks* = 0.0019 m and *Cs*= 0.5 (it can be set from 0.5 to 1) are chosen from Ramponi and Blocken (2012). The surface standard wall functions are used with zero roughness height. Zero static pressure and wall

conditions are applied to the outlet and sidewalls, respectively.

$$K_S = \frac{9.793 y_0}{C_s} \tag{7}$$

Figure 4 illustrates the inlet open terrain time averaged mean velocity and turbulence intensity profiles for turbulence models. The BCs were set using the above Eqs. (2-7), the profiles of the streamwise inlet mean velocity and turbulence intensities are measured at the distance 7D upstream of the building. This shows a good agreement of simulation results with the experiments.

3.2 Solver Setting and Control

All computational simulations were conducted at CFD laboratory, VIT- Chennai. The computational simulations are executed using ANSYS Fluent 18, to resolve the 3D URANS equation with a combination of turbulence models. The velocity-pressure coupling SIMPLE algorithm discretizes the governing equations. The second-order implicit method was used in the transient formulations, wherein the time step size (Δt=Typical element size / Characteristic flow mean wind velocity) $\Delta t = 0.00014$ *s*. For continuity, the convergence was set and attained when all the residuals were scaled and leveled off and reached a least of 10^{-5} and 10^{-6} for *x, y, z* momentum. The assumed residuals were attained and monitored over a considerable period.

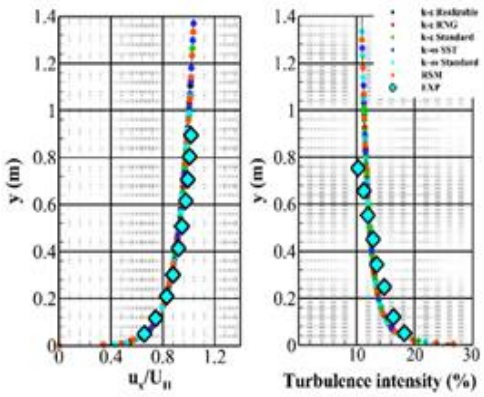

Fig. 4. Inlet open terrain velocity and Turbulence intensity profiles.

3.3 Assessment of URANS turbulence models

The comparisons were made by adopting the Mean Pressure Coefficient ($C_{p\ mean}$) of the setback tall building to analyze the accuracy of CFD prediction of different turbulence models. Pressure coefficients are commonly used for calculating the wind load on a tall building and as a statistical tool to test the accuracy of the CFD turbulence model. The pressure coefficients are measured at the height of *y/H*= 0.475. The mean pressure coefficient is given by:

$$C_{p_{mean}} = \frac{p - p_0}{\frac{1}{2}\rho U_H^2} \tag{8}$$

Where *p* is the pressure extracted from the point at which it needs to be extracted, static pressure at the reference height is p_0, density of air is (1.225 Kg/m3) ρ , U^2_H is the time averaged wind velocity at the reference height of the building.

The RMS pressure coefficients ($C_{p\ rms}$) found from the fluctuating dynamic pressure is given below:

$$C_{p_{r.m.s}} = \frac{\tilde{p}}{\frac{1}{2}\rho U_H^2} \tag{9}$$

Where,

$$\tilde{p} = \left[\frac{1}{T}\int \left[p(t) - \bar{p}\right]^2 dt\right]^{1/2}$$

$$\bar{p} = \frac{1}{T}\int_0^T p(t)dt$$

$\check{p}$ is the rms pressure to the reference dynamic velocity; $\overline{P}$ is the mean pressure obtained for a time *'T'*.

4. RESULTS AND DISCUSSION

4.1 Validation

The performance of the six turbulence models were compared with measured wind tunnel results in terms of $C_{p\ mean}$, $C_{p\ rms}$ and mean aerodynamic coefficients.

Mean pressure coefficients

Figure 5 compares different turbulence models for $C_{p\ mean}$ in terms of R^2 corresponding to CFD turbulence models and the experimental wind tunnel results.

The $C_{p\ mean}$ values are extracted at the height of y/H=0.475. All six models predicted $C_{p\ mean}$ values satisfyingly only for the windward face. Almost all the turbulence models showed similar results (positive values) except the k-ε standard for the windward face of the building. Whereas for the leeward and side faces, significant discrepancies were found in the standard and RNG k-ε turbulence models due to wind shear and vortices compared to all other models. The k-ε models presented the lowest values compared to other turbulence models for the leeward and side face. The k-ω SST and RSM models showed the best wind pressure coefficients compared with other turbulence models.

Root Mean Square pressure coefficient

The comparison of $C_{p\ r.m.s}$ values is made using Eq. (9) for y/H = 0.475 is shown in Fig. 6.

The performance of turbulence models can be revealed from the $C_{p\ r.m.s}$. The RSM turbulence model showed the best performance, especially in reproducing high-pressure fluctuations among all the models. In the k-ε family, the k-ε RNG model showed better results at higher fluctuation zones whereas, in the k-ω family, SST performed comparably well. The predicted $C_{p\ r.m.s}$ values of

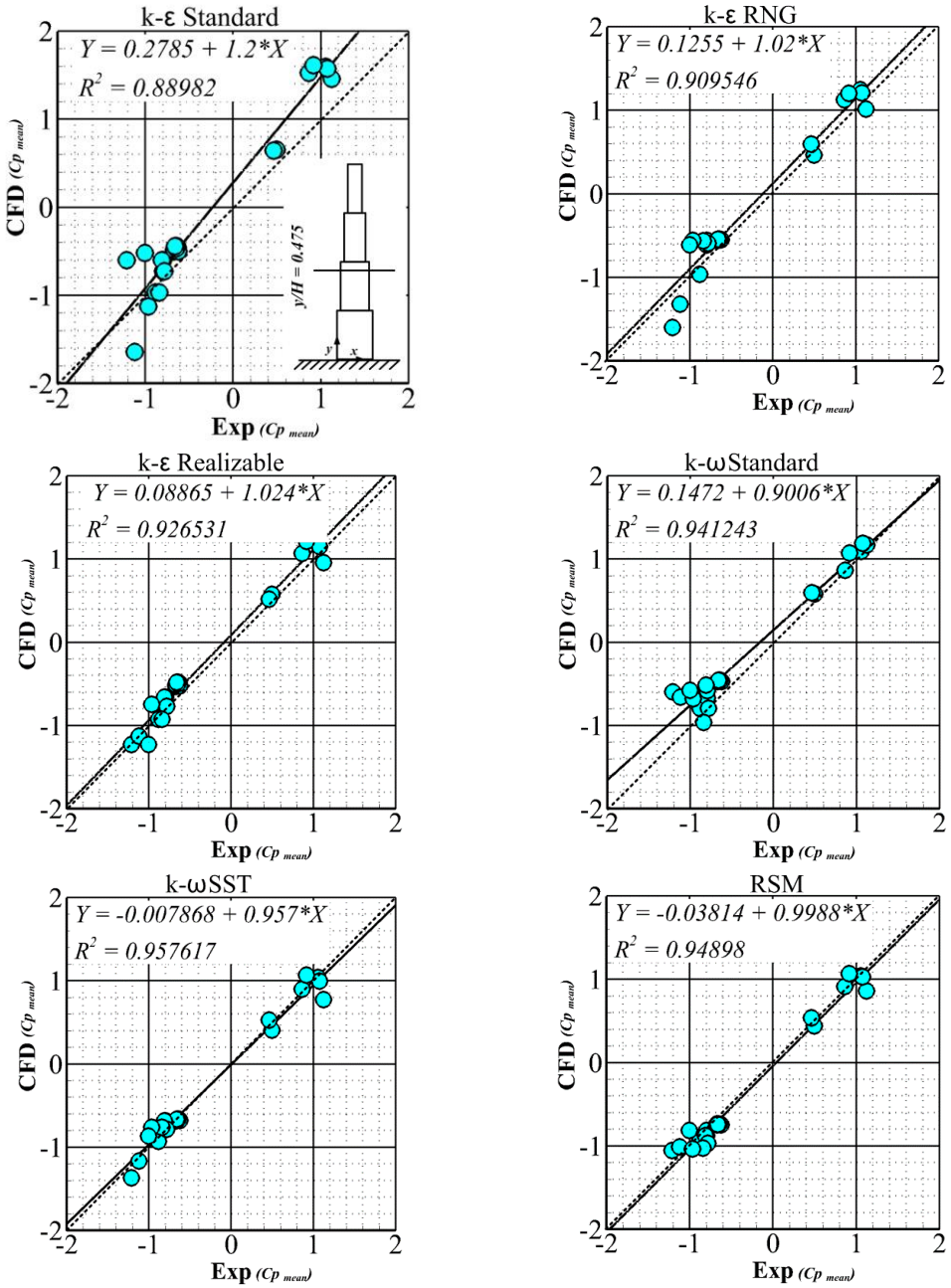

Fig. 5. Comparison of turbulence models with Cp mean of the setback building Root Mean Square pressure coefficient.

other models showed significant discrepancies in their magnitudes with experimental results. These discrepancies demonstrate the dependence of upstream turbulence in fluctuating pressures on tall buildings. Similarly, Daniels *et al.* (2013) and Huang *et al.* (2007) have described a quite complex fluctuating pressure in the upstream turbulence on the surface of a tall building through their computational simulations.

4.2 Wind Flow Field Assessment around the Setback Building on Upstream and Downstream Wake Zones for Various Turbulence Models

Upstream and downstream recirculation velocity profiles are plotted with respect to the building width (D) for various turbulence models and are compared in Fig. 7. The computational models accurately reproduced the up-flow stagnations at four different heights. The stagnation effects were minimum of 1.5 D at y/H=0.875 and a maximum of 5D at 0.125H (y/H= 0.125) upstream of the building. At y/H=0.625, upstream stagnation is fluctuated due to high stagnation pressure on that height; there k-ε Realizable model shows a little higher value. All turbulence models performed un-identical in estimating the size of the recirculation zone. At y/H=0.875, RSM and k-ω SST models estimated wake zone at 2D and other models at 1D downstream. The wake zones are larger at y/H=0.375 and decrease in size towards the height of the building with 5.5D, 4D, and 2.2D for y/H=

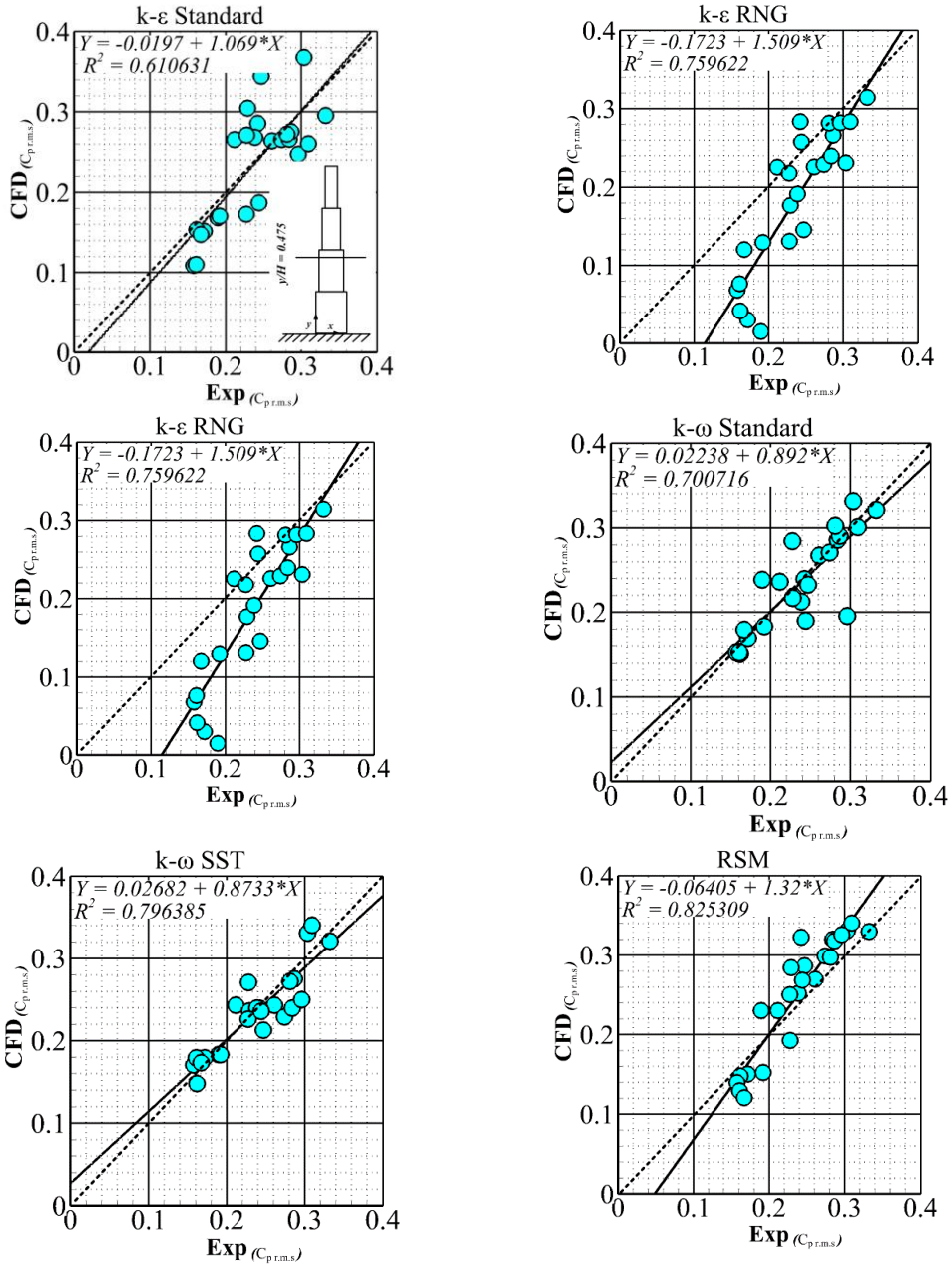

Fig. 6. Comparison of turbulence models with Cp rms of the setback building.

Table 2. Downstream reattachment lengths at different heights for various turbulence models

S. no	Turbulence model	Re-attachment length (x_D/D)			
		$H=0$	$H=0.12$	$H=0.37$	$H=0.62$
1	k-ε Standard	4	2.8	1.8	1
2	k-ε Realizable(REZ)	4.2	2.8	4	1
3	k-ε RNG	5	5.2	2.5	1
4	k- ω Standard	3.5	4	2.5	1.2
5	k- ω SST	3	4	3.4	2
6	RSM	5.2	5.5	4	2

*x_D = *Downstream reattachment length*

0.375, 0.625 and 0.875, respectively. Comparison of the reattachment lengths produced for different turbulence models shows that the RSM model exhibits higher values at the downstream (Table.2). In contrast, for k-ω SST, a lower value was observed in the recirculation wake zone and a rapid velocity gradient at y/H=0.125. This deviation among the models again reveals the difficulty to choose the turbulence model to predict the flow recovery and recirculation zones.

4.3 Computation of Mean Aerodynamic Force Coefficients

Aerodynamic force coefficients are essential for analysing wind-induced building responses. In the resonant responses, the lift force coefficients play a substantial role. Eq. (10) and (11) calculate the

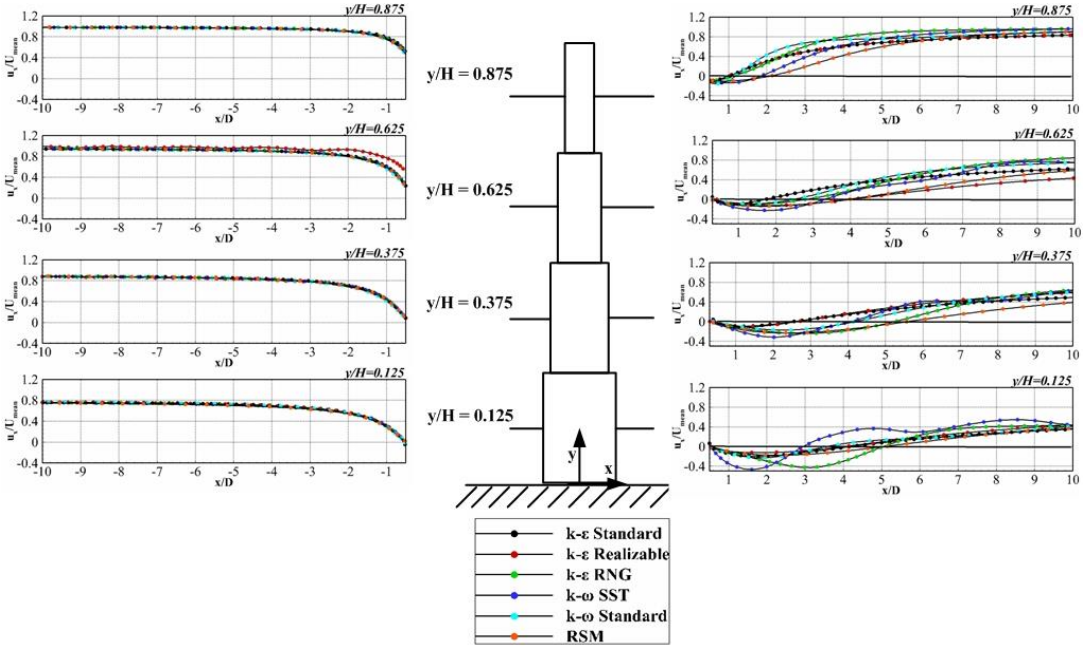

Fig. 7. Comparison of turbulence models of time-averaged upstream and downstream recirculation velocity profile.

mean aerodynamic force coefficients, which are functions of approached open terrain wind flow.

$$C_{Dmean} = \frac{F_D}{\frac{1}{2}\rho U_H^2 D} \tag{10}$$

$$C_{Lmean} = \frac{F_L}{\frac{1}{2}\rho U_H^2 D} \tag{11}$$

Where C_{Lmean} and C_{Dmean} are the mean lift force and drag coefficients, the streamwise wind force is denoted by F_D, the transverse wind force is denoted by F_L, and U^2_H is the reference velocity at the roof of the building (13.6 m /s) and D is the wind projected area parallel to the wind direction. Table.3 compares force coefficients between CFD turbulence models and measured experimental wind tunnel data from the setback building.

Table 3. Comparison of mean aerodynamic coefficients for setback building using various turbulence models

S.no	***Turbulence model***	***CL Mean***	***CD Mean***
1	k-ε Standard	0.059	1.051
2	k-ε Realizable (REZ)	0.062	0.939
3	k-ε RNG	0.054	0.913
4	k- ω Standard	0.042	1.174
5	k- ω SST	0.047	1.309
6	RSM	0.057	1.107
7	**Experiment**	***0.041***	***1.25***

The drag force has a significant association with the distribution of pressure on the leeward and windward faces. In contrast, lift force is associated with the distribution of lateral side of the building. The k-ω turbulence model family has shown better performance when compared to other models. The wind force coefficients have demonstrated reasonable agreement with the experimental value with the RSM model. The k-ε family models have significant discrepancies among other models though it is optimum in some cases of CFD application.

4.4 Comparison of Wind Flow Distribution of the Setback Building under Different Turbulence Models

The assessed turbulence models' mean wind velocity contours and streamlines are presented for the wind flow field around the setback building. The mean wind flow fields are universally comparable for all turbulence models, but the streamlines are not. The mean wind flow pattern for the X-Z plane around the building is shown in Fig.8. These figures show the flow separation at the top and wake zones behind the building. However, there are two differences between them: streamline pattern in the wake zone and degree of recirculated flow shape in the wake zone. The distance of the wake zone for the RSM model is more significant than that for the other turbulence models, similar to the results for reattachment length (x_D/D) in Table 2.

Meanwhile, the other turbulence models predict comparable reattachment lengths. The degree of streamlining varies from model to model. From recirculation and size, it is distinguished that the flow pattern in the wake zone is asymmetric.

The possible impact is the sampling time to obtain the unsteady wall statistics of mean wind velocity. The assessed sampling time of each model t^*=68 ($t^*=\Delta T\ (U_{mean} / U_H)$ t^* is the sampling time, ΔT is the sampling time, U_{mean} is the time averaged inlet velocity and U_H is the velocity at reference height).

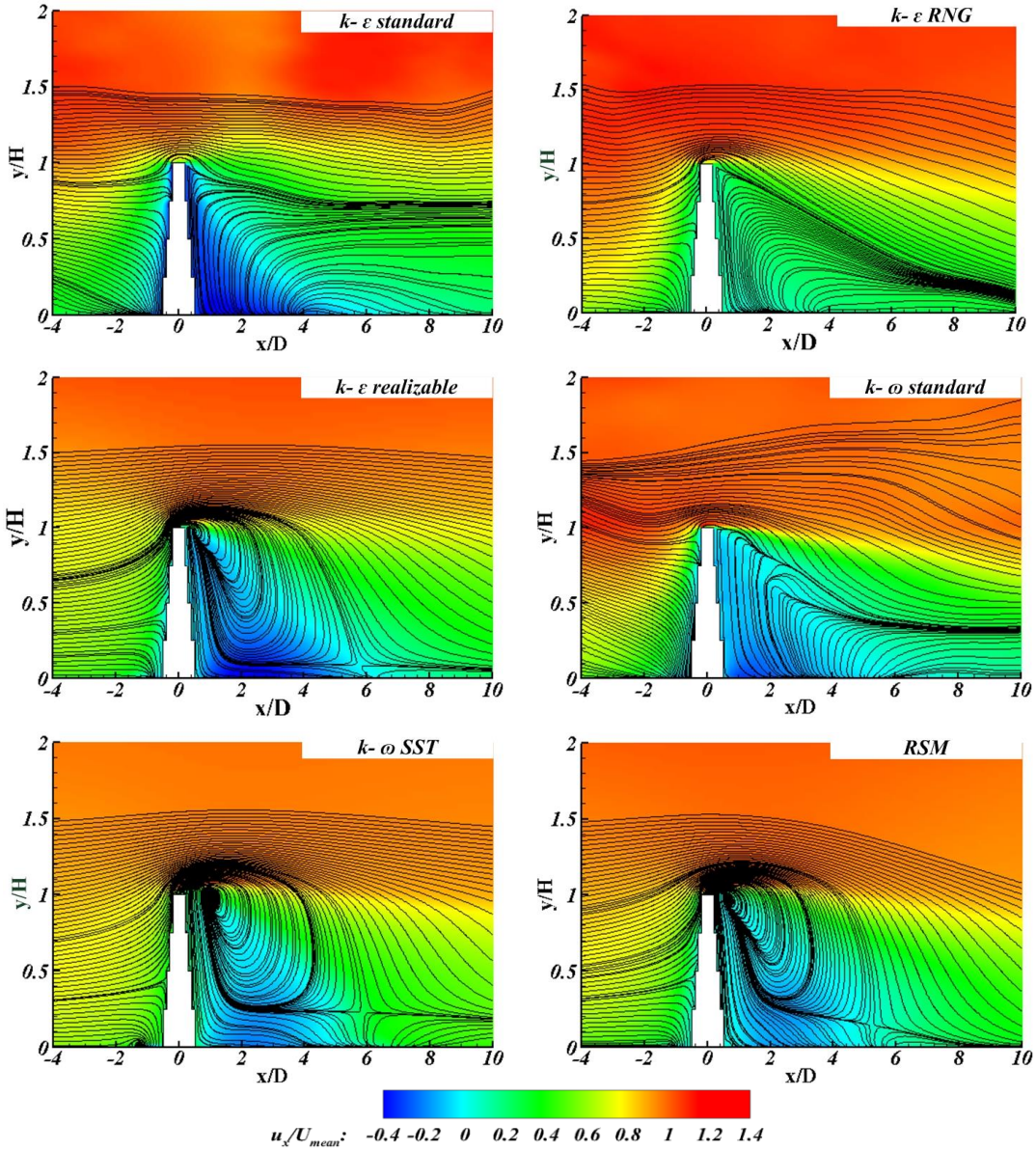

Fig.8. Open terrain wind flow distribution for various CFD turbulence models

The asymmetry of streamline may indicate that choosing an appropriate turbulence model is critical in the URANS approach and worthy for further wind flow studies.

4.5 Comparison of Across Wind Power Spectrum Density with Various Turbulence Models

This section deals with how URANS turbulence models perform across wind spectrum to estimate their efficiency in solving the dominant building wakes. For this purpose, the spectrum is calculated and compared using time-history data of the lift coefficient signals of the setback building. This is made to find the timescale of the energy-containing turbulent eddies in building aerodynamics by Bazdidi-Tehrani *et al.* (2015). The Power Spectral Density (PSD) graphic identifies the frequency with the highest energy unsteady signal. The fluctuating turbulent wind power in any vertical/transverse/longitudinal direction is termed as PSD. This is determined as the square of the flow velocity's Fourier transform divided by the time sample period.It provides energy per unit time per frequency band. Inorder to evaluate the power spectra of the wind, the time histories of lift coefficient data over the building are taken. The PSD signals are presented in Fig. 9. The sample rate is proportional to the time step, Δt= 0.000014, and the duration of the signal is in the order of 68 vortex shedding cycles. The frequency content across wind generated by k-ω STD is the lowermost of all URANS models, bringing in a quick decay of the energy spectra in the low-frequency range. Altogether, the turbulence energy is preserved well for all URANS, especially RSM, k-ε REZ and k-ω SST (See Fig. 9) at lower frequencies.

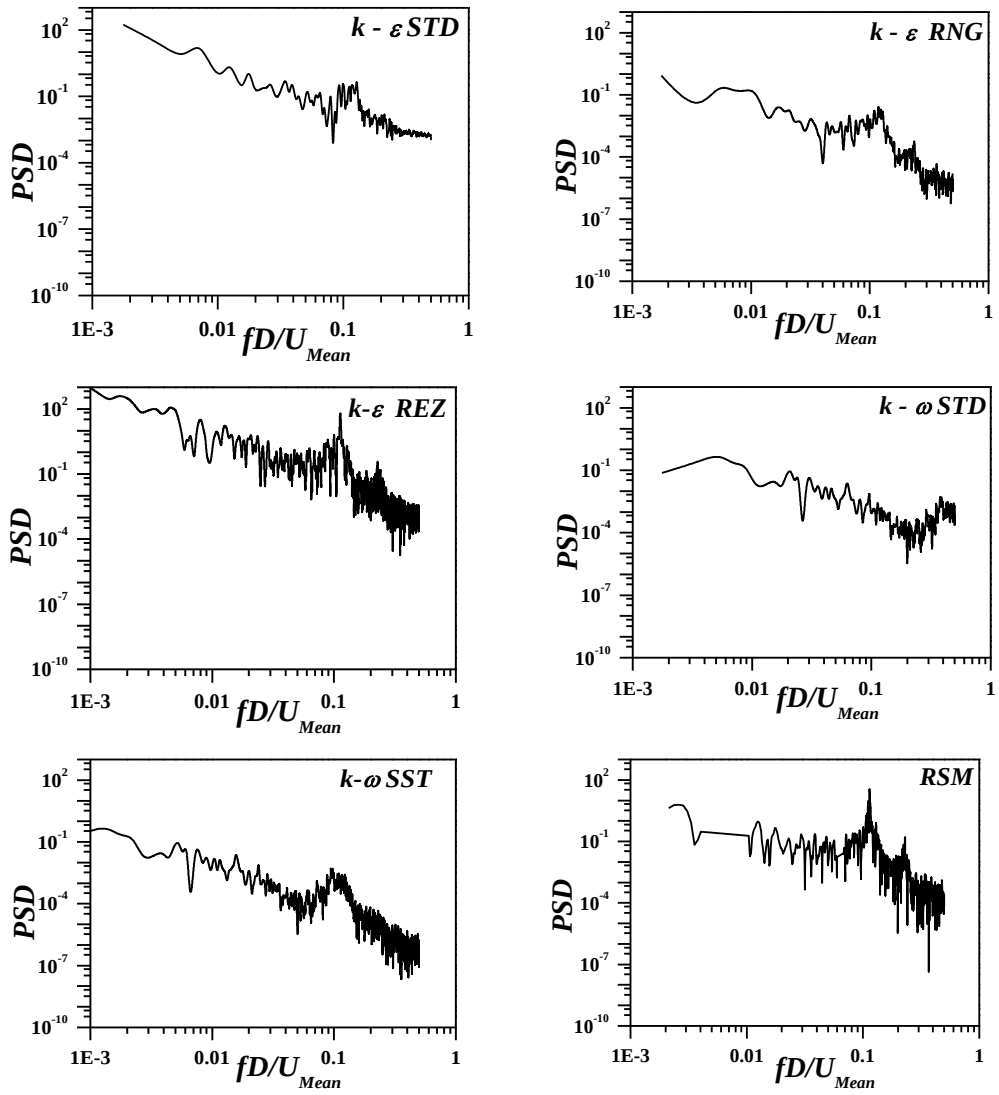

Fig. 9. Across wind flow spectra for various CFD turbulence models.

The k-ε REZ, k- ω SST, and RSM, which follow the temporal history of the across wind, create higher frequency velocity variations. In contrast, the fluctuations caused in the across wind frequency content by the k-ω SST is lesser than that of k-ε REZ. Additionally, the spectra created by the k-ε family show a rapid drop in the high-frequency band, although the k-ε STD and k-ε RNG display distinct behaviours. Lower energy levels predicted by the k-ε RNG and k-ε STD in Fig. 9 indicate an under prediction of wake caused by the lower fluctuations (see Fig. 8). The k-ε REZ model shows that the turbulence energy can be resolved as same as that of RSM effectively. For higher frequencies, the k-ε REZ determines the turbulence energy effectively. In contrast, the k-ε STD and k-ε RNG are incapable of resolving the energy of turbulence to the same extent due to the limitation of these model formulations.

The Strouhal number (fD/U_{Mean}) for URANS models ranges from 0.14 to 0.17. All URANS model evolves towards a general shaped spectrum except k-ω STD; this value corresponds to energy cascades from the higher part of the spectrum to the lower part. The Strouhal number corresponding to the 1:1.5 setback building is equal to 0.145 which is comparable to the well-known literary value for a 1:1 setback building by Tanaka *et al.* (2012). The RSM and k-ε REZ model spectra show a peak of 0.142 and 0.145, respectively. This difference is due to the predominant turbulence effects which leads to more shedding. As a result, k-ε REZ is most suitable for this unsteady feature, while the k-ω SST is appropriate in the initial stage of parametric studies.

Rather than leading to definite peak, the wide range of time and length scales in building wind flow leads to dominating frequency. The ranges of PSD change from model to model due to the small-scale fluctuations produced by the across wind of the building. These fluctions cannot be seen explicitly with any URANS model. These results indicate that it is significant to appropriately assess the energy transfer in the middle of large-scale and small-scale turbulence fluctuations.

4.6 Distribution of Turbulence Kinetic Energy (TKE) among the URANS model

Figure 10 Shows the Turbulence Kinetic Energy (TKE) of the setback building. The TKE measures the amount of energy contained in the turbulence fluctuation. In the wake region, the level of TKE is considerably low for k-ε STD compared with other models. The k-ε STD model underestimated the generation of TKE over the rooftop and its fusion behind the structure. For k-ε RNG, TKE levels are highest at the windward face's impingement shear region and overestimate near the upstream corners. The presence of high turbulence intensity regions (Near the ground) shows less TKE in the low-velocity area for all turbulence models. The same TKE distribution is observed for k-ε REZ in the wake zone. The k-ε RNG over predicted TKE more in upstream and wake regions compared to the k-ε family. These changes may influence turbulence viscosity in the model. In the k-ω STD model, TKE is high in the stagnation region and is similar to k-ε RNG in the strong shear flow region. This shows that k-ω STD under predicts the amount of separation for severe adverse pressure gradient flows. The rooftop TKE formation is feeble, but it is predicted well with unsteady features in k-ω SST in the wake region. Large-scale to small-scale turbulence fluctuations reduce the TKE. In the RSM model, downstream TKE are high compared to other models. In the upstream edges, the distribution is low, revealing that the RSM model modelled wind turbulence well downstream compared to other models. Similarly, the RSM model normal stresses are not assumed isotropic; thus, TKE production is avoided.

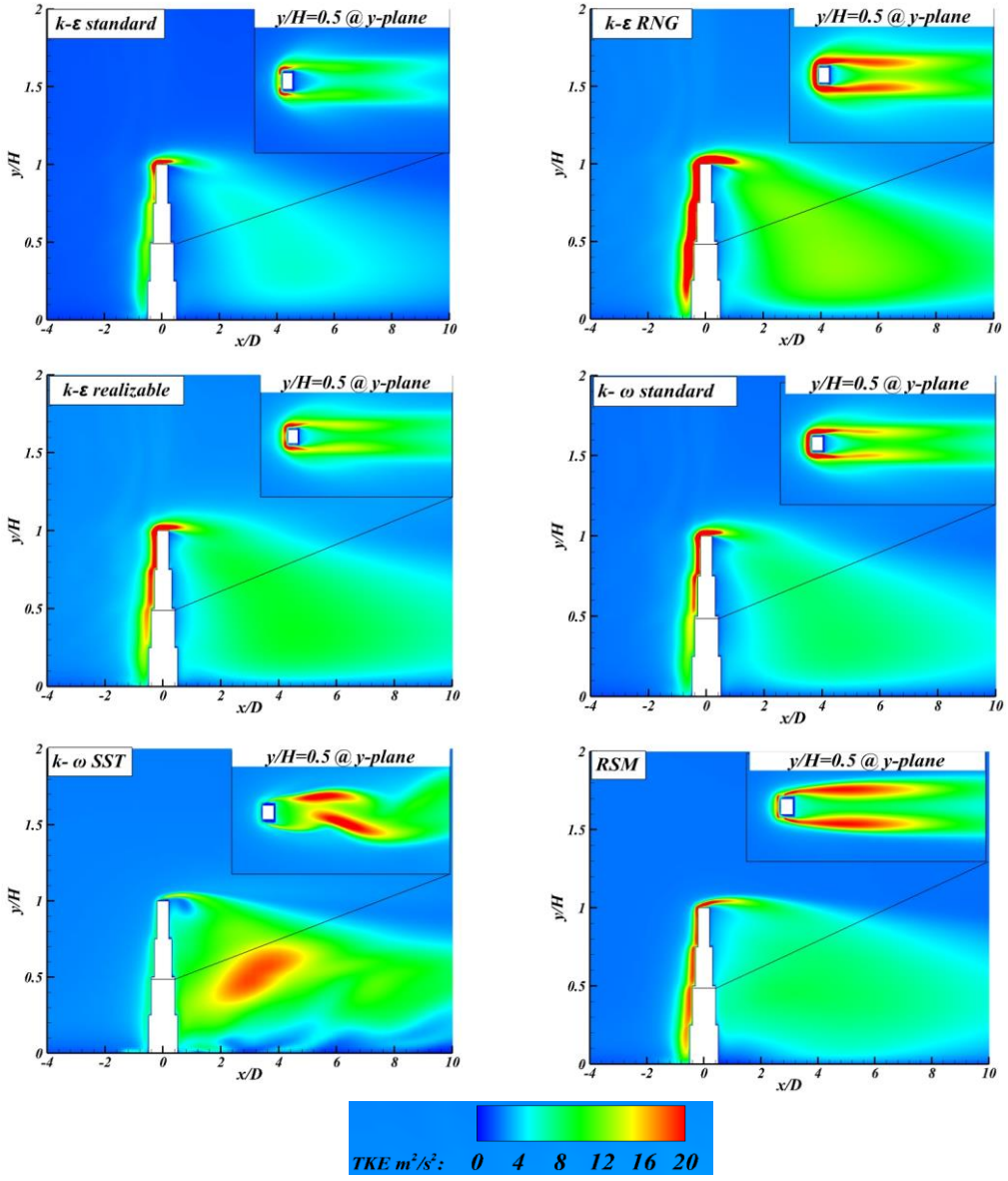

Fig. 10. Contours of TKE for various CFD turbulence models.

4.7 Comparison of vortex structures with various turbulence models

The vortex formations with all turbulence models are compared. Vortex structures behind the building were visualized with the help of the below-defined Eq. (12) called Q- criterion formulae.

$$s_{ij} = \frac{1}{2}\left(\frac{\partial u_i}{\partial x_j} + \frac{\partial u_j}{\partial x_i}\right), r_{ij} = \frac{1}{2}\left(\frac{\partial u_i}{\partial x_j} + \frac{\partial u_j}{\partial x_i}\right) \quad (12)$$

The value of Q is chosen as 0.15 to achieve a preferred flow structure. The time-averaged vortex structures obtained using Q = 0.15 with various turbulence models are shown in Fig. 11 (using fine mesh). It represents the capability of the CFD turbulence models to achieve chaotic large-scale vortices. The k-ω standard and RNG models have captured the trailing vortices downstream, whereas the k-ω standard model failed to predict the horseshoe vortex. k-ε Standard, realizable, and RSM models captured only the arc-like core circulation vortices.

Simultaneously, k-ω SST shows some dissimilarities, particularly in the wake and side separation regions. captured almost all the giant vortex structures were captured by the k-ω SST model especially in the wake zone, extending with the shedding of vortices and capturing the wake expansion and base trailing vortices.

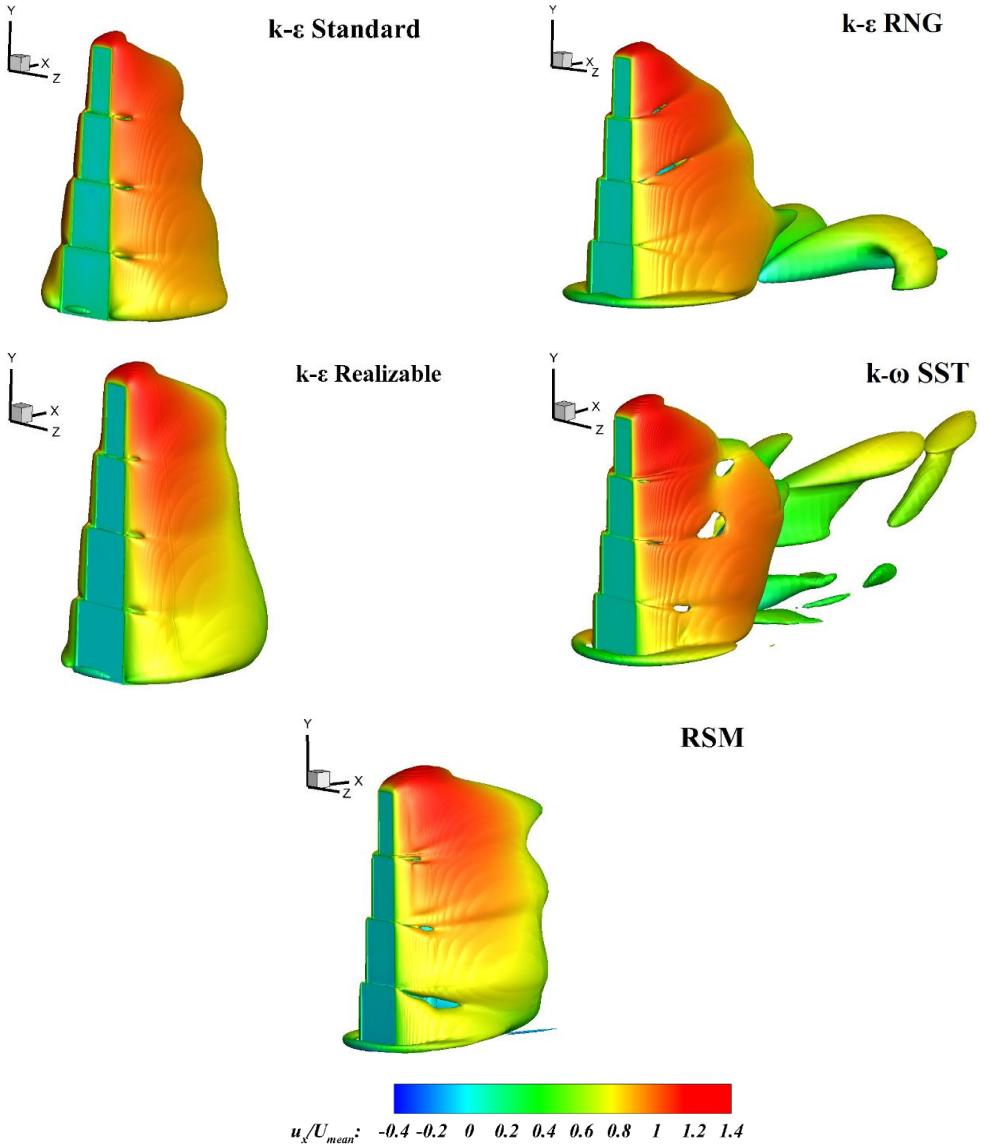

Fig. 11. Iso-surface of various CFD turbulence models.

5. CONCLUSION

The present work aims to understand the performance of URANS models in capturing wind flow features around a building computationally and validate them with wind tunnel results. The URANS models were considered for different assumptions of turbulence flow. Moreover, it was noticed that turbulent terms in the Navies–Stokes equation are vital in predicting results. In this process, evaluation of Cp_{rms}, across wind spectra and iso-surface with URANS models is not common, and these evaluations are not overviewed in earlier studies. These comparisons are significant while choosing the CFD turbulence model for assessing the fluctuating wind force and flow around tall buildings. From this evaluation, the following important conclusions can be derived.

- The mean pressure coefficients and fluctuating wind pressures are extracted at y/H=0.475 height for all the cases. Among all the models, the k–ω SST model in predicting the mean quantities with the least discrepancies showed the best performance. Whereas the RSM turbulence model performed better on capturing fluctuating pressure. K–ω SST demonstrated the second-best performance.
- A better agreement was observed on upstream wind velocities, while some discrepancies were noticed at downstream velocity. It was also noted that each model has a different performance with each case.
- The k–ω family and RSM turbulence models were assessed well for the aerodynamic coefficient, while k–ε realizable and standard models displayed a large discrepancy.
- The magnitude of recirculation length and streamline patterns varied from model to model, especially in the wake zone. This shows the significance of sampling time in the unsteady phenomenon.
- The peak frequency of across wind power spectra obtained by the URANS was in agreement with the literature. The Strouhal number of the RSM and k-ε REZ model showed a peak of 0.142 and 0.145, respectively.
- The k–ω SST considerably undervalued the TKE compared to other models. The flow separation was over-estimated significantly, despite their production of periodic fluctuation around the corners of the building.
- In the k– ε family, k-ε RNG captured the tail vortices, and the remaining turbulence models captured the arc vortices as same as other models. The unsteady phenomenon connecting with Q-criterion to capture the vortex structure in the k–ω family, remarkably the k–ω SST performed well and captured most of the large vortices among these models. Overall, k–ω SST is most reliable in predicting mean flows and unsteady phenomena with less computational time and resources for complex environmental wind flow around the building.

REFERENCES

Bazdidi-Tehrani, F., A. Mohammadi-Ahmar, M. Kiamansouri and M. Jadidi (2015). Investigation of various non-linear eddy viscosity turbulence models for simulating flow and pollutant dispersion on and around a cubical model building. In *Building Simulation* 8(2), 149-166).

Blocken, B. (2018). LES over RANS in building simulation for outdoor and indoor applications: a foregone conclusion? *Building Simulation* 11(5), 821-870).

Blocken, B., W. D. Janssen and T. van Hooff (2012). CFD simulation for pedestrian wind comfort and wind safety in urban areas: General decision framework and case study for the Eindhoven University campus. *Environmental Modelling & Software* 30, 15-34.

Blocken, B., T. Stathopoulos and J. Carmeliet (2007). CFD simulation of the atmospheric boundary layer: wall function problems. *Atmospheric Environment* 41(2), 238-252.

Blocken, B., T. Stathopoulos, J. Carmeliet and J. L. Hensen (2011). Application of computational fluid dynamics in building performance simulation for the outdoor environment: an overview. *Journal of Building Performance Simulation* 4(2), 157-184.

Cebeci, T. and P. Bradshaw (1977). *Momentum transfer in boundary layers*. Washington DC,319-321 Hemisphere.

Daniels, S. J., I. P. Castro and Z. T. Xie (2013). Peak loading and surface pressure fluctuations of a tall model building. *Journal of Wind Engineering and Industrial Aerodynamics* 120, 19-28.

Franke, J., A. Hellsten, K. H. Schlünzen and B. Carissimo (2007). *Best practice guideline for the CFD simulation of flows in the urban environment-a summary*. In 11th Conference on Harmonisation within Atmospheric Dispersion Modelling for Regulatory Purposes, Cambridge, UK, July 2007. Cambridge Environmental Research Consultants.

Fluent, A. N. S. Y. S. (2017). 18.0 ANSYS Fluent theory guide 18.0. Ansys Inc.

Hanjalić, K. and S. Kenjereš (2008). Some developments in turbulence modeling for wind and environmental engineering. *Journal of*

Wind Engineering and Industrial Aerodynamics 96(10-11), 1537-1570.

Hassan, S., M. Molla, P. Nag, N. Akter and A. Khan (2021). Unsteady RANS simulation of wind flow around a building shape obstacle. *Building Simulation*, 1-22.

Huang, S., Q. S. Li and S. Xu (2007). Numerical evaluation of wind effects on a tall steel building by CFD. *Journal of Constructional Steel Research* 63(5), 612-627.

Hussain, A. K. M. F. and W. C. Reynolds (1970). The mechanics of an organized wave in turbulent shear flow. *Journal of Fluid Mechanics* 41(2), 241-258.

Iqbal, Q. M. Z. and A. L. S. Chan (2016). Pedestrian level wind environment assessment around group of high-rise cross-shaped buildings: Effect of building shape, separation and orientation. *Building and Environment* 101, 45-63.

Joubert, E. C., T. M. Harms and G. Venter (2015). Computational simulation of the turbulent flow around a surface mounted rectangular prism. *Journal of Wind Engineering and Industrial Aerodynamics* 142, 173-187.

Launder, B. E. and D. B. Spalding (1974). The Numerical Computation of Turbulent Flows. Computer Methods in Applied Mechanics and Engineering, 3, 269-289.

Li, T., D. Qin and J. Zhang (2019). Effect of RANS turbulence model on aerodynamic behavior of trains in crosswind. *Chinese Journal of Mechanical Engineering* 32(1), 1-12.

Mochida, A. and I. Y. Lun (2008). Prediction of wind environment and thermal comfort at pedestrian level in urban area. *Journal of wind engineering and industrial aerodynamics* 96(10-11), 1498-1527.

Mochida, A., Y. O. S. H. I. H. I. D. E. Tominaga, S. Murakami, R. Yoshie, T. Ishihara and R. Ooka (2002). Comparison of various k-ε models and DSM applied to flow around a high-rise building-report on AIJ cooperative project for CFD prediction of wind environment. *Wind and Structures* 5(2_3_4), 227-244.

Paul, R. and S. K. Dalui (2016). Wind effects on 'Z'plan-shaped tall building: a case study. *International Journal of Advanced Structural Engineering* 8(3), 319-335.

Rahmatmand, A., M. Yaghoubi, E. G. Rad, M. M. Tavakol (2014). 3D experimental and numerical analysis of wind flow around domed-roof buildings with open and closed apertures. *Building simulation* 7(3), 305-319.

Rajasekarababu, K. B. and G. Vinayagamurthy (2019). Experimental and computational simulation of an open terrain wind flow around a setback building using hybrid turbulence models. *Journal of Applied Fluid Mechanics* 12(1), 145-154.

Rajasekarababu, K. B. and G. Vinayagamurthy (2020). CFD validation of wind pressure distribution on a tall building under the influence of upstream terrain. *Progress in Computational Fluid Dynamics, an International Journal* 20(5), 284-298

Rajasekarababu, K. B., G. Vinayagamurthy, S. S. Rajan (2016). Numerical simulation of the wind environment around a setback building: An evaluation of turbulence models. In: Proceedings of the 8th National Conference on Wind Engineering, Varanasi, India.

Ramponi, R. and B. Blocken (2012). CFD simulation of cross-ventilation for a generic isolated building: impact of computational parameters. *Building and environment* 53, 34-48.

Tanaka, H., Y. Tamura, K. Ohtake, M. Nakai, Y. C. Kim (2012). Experimental investigation of aerodynamic forces and wind pressures acting on tall buildings with various unconventional configurations. *Journal of Wind Engineering and Industrial Aerodynamics* 107, 179-191.

Tominaga, Y. (2015). Flow around a high-rise building using steady and unsteady RANS CFD: Effect of large-scale fluctuations on the velocity statistics. *Journal of Wind Engineering and Industrial Aerodynamics* 142, 93-103.

Tominaga, Y. and T. Stathopoulos (2013). CFD simulation of near-field pollutant dispersion in the urban environment: A review of current modeling techniques. *Atmospheric Environment* 79, 716-730.

Tominaga, Y., A. Mochida, R. Yoshie, H. Kataoka, T. Nozu, M. Yoshikawa and T. Shirasawa (2008). AIJ guidelines for practical applications of CFD to pedestrian wind environment around buildings. *Journal of Wind Engineering and Industrial Aerodynamics* 96(10-11), 1749-1761.

Toparlar, Y., B. Blocken, P. V. Vos, G. J. F. Van Heijst, W. D. Janssen, T. van Hooff, H. Montazeri and H. J. P. Timmermans (2015). CFD simulation and validation of urban microclimate: A case study for Bergpolder Zuid, Rotterdam. *Building and Environment* 83, 79-90.

Vatin, N., S. Isaev, S. Guvernyik, V. Gagarin, B. Basok and Y. Zhukova (2014). Architectural building aerodynamics of tall structures with the bleeding effect and wind energy selection. In *The International Scientific Conference "Innovative Materials, Structures and Technologies"* (193-197).

Wintergerste, T., M. Casey and A. G. Hutton (2002). The Best Practice Guidelines for CFD: A European Initiative on Quality and Trust (Keynote). In *ASME Pressure Vessels and*

Piping Conference 46598 (1-9).

Yagmur, S., S. Dogan, M. H. Aksoy and I. Goktepeli (2020). Turbulence modeling approaches on unsteady flow structures around a semi-circular cylinder. *Ocean Engineering* 200, 107051.

Yuan, W., Z. Wang, H. Chen and K. Fan (2017). Numerical analyses of aerodynamic characteristics of integrated L-shaped high-rise building. *Advances in Engineering Software* 114, 144-153.

Zhang, D. (2017). Comparison of various turbulence models for unsteady flow around a finite circular cylinder at Re= 20000. In Journal of Physics: Conference Series 910(1) 012027.

Zhang, Y., W. G. Habashi and R. A. Khurram (2015). Predicting wind-induced vibrations of high-rise buildings using unsteady CFD and modal analysis. *Journal of Wind Engineering and Industrial Aerodynamics* 136, 165-179.